

## Electronic transport in lightly doped CoSb<sub>3</sub>

D. Mandrus, A. Migliori, T. W. Darling, M. F. Hundley, E. J. Peterson, and J. D. Thompson  
*Los Alamos National Laboratory, Los Alamos, New Mexico 87545*

(Received 16 January 1995)

We report resistivity, Hall coefficient, and Seebeck coefficient measurements on a very lightly doped ( $1/R_H e = 7.0 \times 10^{16}$  holes/cm<sup>3</sup>) single crystal of CoSb<sub>3</sub>. The low-temperature resistivity is semiconducting, with a gap  $E_g = 580$  K ( $\approx 50$  meV). At high temperatures another energy scale is apparent, with a characteristic energy  $E_g = 3650$  K ( $\approx 0.31$  eV). The presence of two energies is consistent with a recent band-structure calculation performed by Singh and Pickett. The Hall coefficient is large and positive, as expected for a lightly doped *p*-type semiconductor. Below 200 K, the Hall mobility  $R_H \sigma$  varies as  $T^{3/2}$ , indicating that ionized impurity scattering is the dominant scattering mechanism. The Hall mobility peaks at 250 K at a value of  $1940$  cm<sup>2</sup> V<sup>-1</sup> sec<sup>-1</sup>. The Seebeck coefficient is small at low temperature, and increases smoothly until it attains a value of  $225$   $\mu$ V/K at 300 K; its temperature dependence is also consistent with ionized impurity scattering. A detailed structural refinement on our crystals gives a lattice parameter of  $9.03573(3)$  Å, with evidence for little or no site disorder.

### I. INTRODUCTION

Skutterudite tri-antimonides, with the general formula (Co,Rh,Ir)Sb<sub>3</sub>, have attracted attention recently<sup>1-4</sup> because of their promise for use in thermoelectric applications. Desirable qualities for thermoelectric materials include a large Seebeck coefficient  $S$ , a large electrical conductivity  $\sigma$ , and a small thermal conductivity  $\kappa$ . These quantities determine the so-called thermoelectric figure of merit,  $Z = S^2 \sigma / \kappa$ . The main problem in the study of thermoelectrics is to find materials with very high values of  $Z$ , or, more precisely, high values of  $ZT$  over the operating temperature range. Skutterudite tri-antimonides are attractive because they have relatively low thermal conductivities, and high electrical conductivities due to the extremely mobile holes in these materials. In a recent study,<sup>4</sup> Slack and Tsoukala estimated that the lattice conductivity of IrSb<sub>3</sub> could be reduced by a factor of 40 without seriously degrading the electrical conductivity. If this reduction could be achieved, then  $ZT$  values of 2 or 3 times the current maximum would be within reach.

Very recently, Singh and Pickett<sup>3</sup> (SP) performed detailed band-structure calculations on a number of skutterudites, including IrSb<sub>3</sub> and CoSb<sub>3</sub>. SP found that in CoSb<sub>3</sub> a pseudogap forms around the Fermi level, and that a single band crosses the pseudogap and forms a direct 50-meV gap at the  $\Gamma$  point. SP also found that in the constant scattering time approximation the hole mobility  $\mu_H$ , normally independent of the carrier density  $n$ , varies as  $n^{-1/3}$  in both CoSb<sub>3</sub> and IrSb<sub>3</sub>; furthermore, the degenerate Seebeck coefficient was found to have a different doping dependence than a normal parabolic band.

In order to test some of these predictions, we prepared very lightly doped single crystals of CoSb<sub>3</sub>. It was important to prepare pure samples so that impurity band conduction did not obscure the low-temperature transport

properties. We measured the resistivity, Hall coefficient, and Seebeck coefficient on the same crystal, and found that CoSb<sub>3</sub> is indeed a narrow-gap semiconductor, and that the gap is about 50 meV. We also found that ionized impurity scattering is the dominant scattering mechanism in our crystals. A simple analysis yields a very light hole mass of  $m^* = 0.011 m_e$ ; this estimate is about an order of magnitude smaller than estimates made assuming acoustic-phonon scattering. Although the carrier mobility appears to increase with decreasing carrier concentration, it is unlikely that the  $n^{-1/3}$  variation, calculated in the constant scattering time approximation, is obeyed in real samples. Similarly, it was not meaningful to compare the measured Seebeck coefficient to the prediction of SP, which also was calculated assuming a constant scattering time.

### II. CRYSTAL GROWTH

Single crystals of CoSb<sub>3</sub> were grown from an Sb-rich melt as follows. Very thin flakes of 99.998% Co were combined with 99.9999% Sb shot in the molar ratio Co:Sb = 1:6.7. The materials were sealed under vacuum in a quartz tube, heated to 1150°C, and allowed to soak at this temperature for 24 h. The temperature was then ramped from 1150 to 900°C at 30°C/h, and from 900 to 650°C at 16.5°C/h. At 650°C, the excess flux was spun off as described by Fisk and Remeika.<sup>5</sup> The resulting crystals were about 1–4 mm on a side, shiny, and well faceted. Before performing the measurements, a small amount of remaining flux was removed from the crystals by etching them in a solution of H<sub>2</sub>O:HNO<sub>3</sub>:HF = 10:5:1. The crystals were characterized with magnetic susceptibility, powder x-ray diffraction, and electronic transport. The magnetic susceptibility was diamagnetic, and varied from  $-8.9 \times 10^{-5}$  emu/mol at low temperature to  $-8.0 \times 10^{-5}$  emu/mol at room temperature. The other measurements are discussed below.

TABLE I. Fractional coordinates and isotropic temperature factors  $U_{\text{iso}}$  with estimated standard deviations in parentheses. Footnotes a–d denote comparisons to previous work.

	$x$	$y$	$z$	$U_{\text{iso}} (\times 10^{-2} \text{ \AA}^2)$
Co	0.25	0.25	0.25	0.85(8) <sup>a</sup> 0.456(4) <sup>b</sup> 0.202(4) <sup>c</sup>
Sb	0.0	0.334 8(1) <sup>a</sup> 0.335 37(4) <sup>b</sup> 0.335 66(5) <sup>c</sup> 0.335 (1) <sup>d</sup>	0.157 0(1) <sup>a</sup> 0.157 88(4) <sup>b</sup> 0.158 63(5) <sup>c</sup> 0.160 (2) <sup>d</sup>	1.00(3) <sup>a</sup> 0.637(4) <sup>b</sup> 0.555(5) <sup>c</sup>

<sup>a</sup>This work.

<sup>b</sup>Schmidt, Kliche, and Lutz (Ref. 8), single crystal, chemical vapor transport, Cl as carrier.

<sup>c</sup>Schmidt, Kliche, and Lutz (Ref. 8), single crystal, recrystallization in the presence of I.

<sup>d</sup>Kjekshus and Rakke (Ref. 9), powder.

### III. STRUCTURAL REFINEMENT

The skutterudite structure (bcc, space group  $Im\bar{3}$ , prototype CoAs<sub>3</sub>) contains eight formula units per cell, and may be regarded as consisting of planes of Co atoms with squares of Sb atoms arranged between the planes.<sup>6</sup> Because of the unusually wide scatter in the literature values of the lattice parameter, we performed a rather complete structural refinement on our crystals.

The sample, consisting of small crystals of CoSb<sub>3</sub>, was ground thoroughly using an agate mortar and pestle, after which silicon standard SRM 640b was blended in. This mixture was poured on top of a quartz zero background that had been lightly coated with silicone grease. Excess powder was removed by softly tapping the sample holder on edge, leaving approximately a monolayer of powder particles coating the quartz plate. Powder x-ray diffraction data were collected using a Scintag XDS2000 theta-theta powder diffractometer equipped with a graphite monochromator in conjunction with a scintillation detector. The sample was spun during data collection. Two data sets were collected: (1) a step scan from 20° to 90°  $2\theta$  with a step size of 0.02° and a count time of 7 s, and (2) a step scan from 70° to 135°  $2\theta$  with a step of 0.04° and a count time of 14 s. The resulting data sets were analyzed simultaneously by the Reitveld method using the computer program GSAS (Generalized Structural Analysis System).<sup>7</sup> A pseudo-Voigt function was used to fit the Bragg diffraction peaks and a cosine Fourier series with three coefficients was used to model the background. Starting values for atomic positions and the unit-cell parameter for CoSb<sub>3</sub> were obtained from Schmidt, Kliche, and Lutz.<sup>8</sup> Antimony metal (presumably from Sb flux sticking to the crystals) was found as a minor impurity in the x-ray diffraction pattern and was included in the refinement. To obtain an accurate unit-cell parameter for CoSb<sub>3</sub>, the silicon lattice parameter was fixed at its certified value of 5.43094 Å and the sample displacement, sample transparency profile parameters, and the diffractometer zero point were allowed to vary. When convergence was achieved, these values were fixed for the silicon standard, antimony, and CoSb<sub>3</sub>, taking into account systematic errors present in the data sets. The lat-

tice parameter for CoSb<sub>3</sub> was then refined. The  $Lx$  and  $Ly$  profile parameters were refined for CoSb<sub>3</sub>, Si, and Sb, and showed essentially no size or strain effects for CoSb<sub>3</sub> when compared to previously refined values for LaB<sub>6</sub> profile standard SRM 660. In contrast, the profile parameters for elemental Sb showed a large component of nonuniform strain. For CoSb<sub>3</sub>, Co and Sb site occupancies were refined separately, as these parameters were somewhat correlated. These parameters refined to values very close to 1.0, indicating little or no atomic disorder, and were left fixed at 1.0 for the final refinement. The results of the CoSb<sub>3</sub> atomic parameter refinement and comparisons to previous studies are presented in Table I; lattice constants are presented in Table II.

### IV. ELECTRONIC TRANSPORT

Resistivity, Hall effect, and thermopower measurements were performed on the same single crystal. The high-temperature resistivity measurements were performed last because measurements on other crystals showed that heating the crystals to temperatures greater than 200 °C produced irreversible changes in the resistivi-

TABLE II. Lattice constant of CoSb<sub>3</sub>. Footnotes a–e denote comparisons to previous work. Goodness of fit criteria: reduced chi-squared: 2.439, weighted residual error, wRp: 0.1480, unweighted residual error, Rp: 0.1067.

Lattice parameter (Å)
9.035 73(3) <sup>a</sup>
9.038 5(3) <sup>b</sup>
9.077 5(6) <sup>c</sup>
9.034 7(6) <sup>d</sup>
9.035 6(6) <sup>e</sup>

<sup>a</sup>This work.

<sup>b</sup>Schmidt, Kliche, and Lutz (Ref. 8), single crystal, chemical vapor transport, Cl as carrier.

<sup>c</sup>Schmidt, Kliche, and Lutz (Ref. 8), single crystal, recrystallization in the presence of I.

<sup>d</sup>Kjekshus and Rakke (Ref. 9), powder.

<sup>e</sup>Schmidt, Kliche, and Lutz (Ref. 8), powder.

ty, and, in at least one case, destroyed the low-temperature semiconducting behavior of the sample.

The resistivity measurements were performed using a dc linear four-probe method; the current was reversed at each temperature to eliminate thermal voltages. Platinum wire (25  $\mu\text{m}$  diameter) and Dupont 4929 silver epoxy were used to make contacts to the sample. The sample dimensions were  $2.5 \times 1.0 \times 0.2 \text{ mm}^3$ . Low currents (10–100  $\mu\text{A}$ ) were used for the measurements because in some samples breakdown effects (presumably due to interband tunneling) were observed at low temperatures. These effects were not studied. For the high-temperature measurements, Epotek H20E silver epoxy was used for the contacts, and the measurements were performed in an argon atmosphere.

The Hall measurements were performed in a constant magnetic field of 20 kOe. At each temperature, the sample was rotated  $180^\circ$  and the current reversed in order to eliminate misalignment and thermal voltages, respectively. Checks were made at several temperatures to ensure that the Hall voltage was linear in current, but no effort was made to establish the magnetic field dependence of the Hall coefficient. The Seebeck coefficient was measured using gold wires (25  $\mu\text{m}$  diameter), a single heater, and a chromel-constantan reference thermocouple. Temperature gradients from 0.1% to 1% of the ambient temperature were established across the sample, and the thermoelectric voltage  $\Delta V$  was measured at each gradient  $\Delta T$ . The Seebeck coefficient  $dV/dT$  was determined by fitting the  $\Delta V$  versus  $\Delta T$  data to a straight line. The data were corrected for the small absolute thermopower of gold.

In Fig. 1 we plot the resistivity, from 5 to 680 K, of the  $\text{CoSb}_3$  crystal used in this study. Although the high-temperature portion of the resistivity resembles that measured by others,<sup>10,11</sup> the low-temperature portion is strikingly different, in that, to the best of our knowledge, the low-temperature semiconducting behavior has not been previously observed.<sup>11,12</sup> We attribute our successful observation of the low-temperature semiconducting

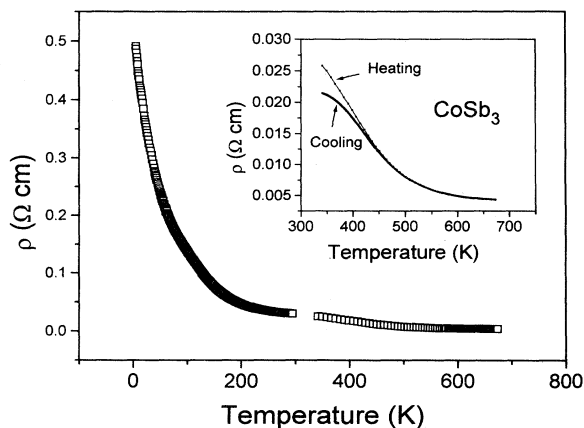


FIG. 1. Resistivity of  $\text{CoSb}_3$ . The inset shows the high-temperature portion of the data. Note that after heating the resistivity does not fully recover. We attribute this to partial decomposition of the sample (see text).

behavior to the high purity of the starting materials, and particularly the Co, used; other crystals, grown using the same technique but with slightly less pure Co (99.95%), did not display the semiconducting behavior. In the inset to Fig. 1 we show the high-temperature portion of the data. Note that after heating, the sample became less resistive; this behavior was observed in several samples, and we attribute it to a partial decomposition of the sample into  $\text{CoSb}_2$  and Sb—both with lower resistivities than  $\text{CoSb}_3$ . Since a similar decomposition was also observed in  $\text{IrSb}_3$ ,<sup>13</sup> it may point to serious difficulties in the use of skutterudite tri-antimonides at high temperatures.

In Fig. 2 we plot  $\ln(\rho)$  versus  $1/T$  for the same data as in Fig. 1. The dotted and dashed lines are fits to the equation  $\rho = \rho_0 \exp(\Delta/T)$ , where the semiconducting energy gap  $E_g = 2\Delta$ . Two energy scales are readily apparent: a lower scale, representing an energy gap of 580 K ( $\approx 50 \text{ meV}$ ), and an upper scale, representing an energy gap of 3650 K ( $\approx 0.31 \text{ eV}$ ). This behavior is in reasonable agreement with a recent band-structure calculation of  $\text{CoSb}_3$  performed by Singh and Pickett,<sup>3</sup> in which they predict a 50-meV semiconducting gap flanked by two large peaks in the density of states separated by 0.5 eV. Our estimate of 0.31 eV for the pseudogap is considerably lower than a previous estimate of 0.50 eV,<sup>10</sup> but in good agreement with a recent estimate of 0.35 eV.<sup>14</sup> Interestingly, optical measurements on a crystal of  $\text{CoSb}_3$  grown by vapor transport showed no evidence of a semiconducting energy gap of any kind.<sup>12</sup>

In Fig. 3 we plot the Hall coefficient  $R_H$  versus  $T$  measured on the same crystal used for the resistivity measurements. The data divide naturally into three regions: (1) the sharp rise from 5 to 50 K, (2) the gentle rise from 60 to 150 K, and (3) the rather steep fall from 150 to 300 K. We can understand the behavior of the Hall coefficient in these three regions as follows. In region 1,  $R_H$  is consistent with the onset of impurity band conduction as  $T$  is decreased below 60 K. Similar behavior was observed in Hall effect measurements on many other semiconductors,

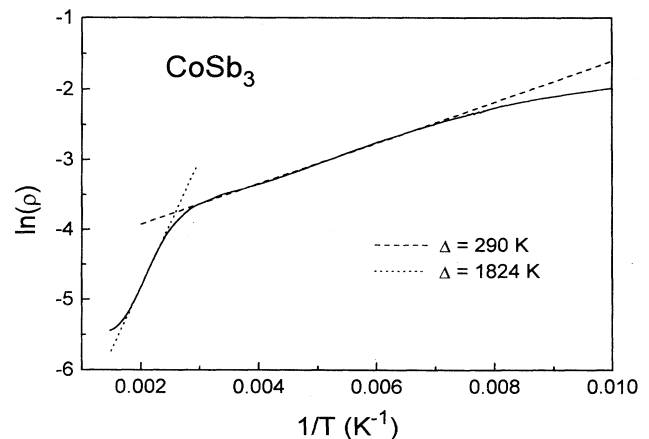


FIG. 2. Solid line, natural log of the resistivity vs temperature for  $\text{CoSb}_3$ . Dotted and dashed lines, fit (over an appropriate temperature range) to the equation  $\rho = \rho_0 \exp(\Delta/T)$ . Two energy scales are readily apparent.

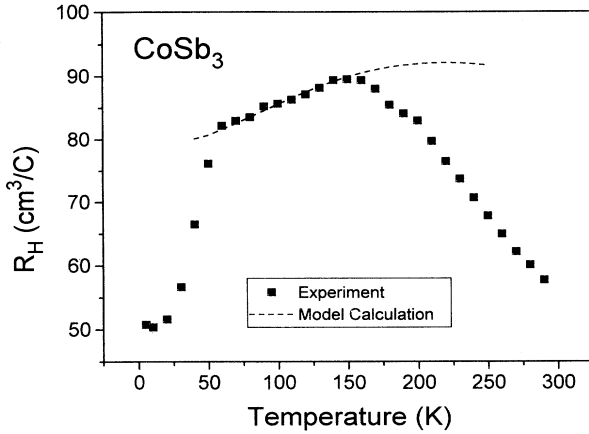


FIG. 3. Hall coefficient vs temperature for CoSb<sub>3</sub>. The dashed line represents a model calculation assuming a single type of carrier, parabolic bands, and scattering from ionized impurities (see text).

and we direct the reader to the literature for details.<sup>15,16</sup> In region 2 the Hall coefficient is relatively constant, which is just what we expect in the saturation, or exhaustion, regime in which conduction takes place via ionized impurities whose number density is hardly changing. Finally, region 3 represents the onset of intrinsic conduction, in which the number of carriers thermally excited across the semiconducting energy gap begins to overwhelm the number of carriers due to ionized impurities. This interpretation is supported by the resistivity data, in that the resistivity deviates from simply activated behavior below about 150 K.

Also plotted in Fig. 3 is a model calculation of the Hall coefficient assuming a single parabolic band and scattering from ionized impurities. The assumption of ionized impurity scattering will be justified below. In this model, the carrier density is given by<sup>17</sup>

$$n = \frac{4\pi(2m^*k_B T)^{3/2}}{h^3} F_{1/2}(E_F^*), \quad (1)$$

where  $m^*$  is the carrier effective mass,  $E_F^* = E_F/k_B T$  is the reduced Fermi energy (or reduced chemical potential), and  $F_m$  is a Fermi-Dirac integral. The Hall coefficient for this model is given by<sup>17</sup>

$$R_H = \frac{3F_{1/2}F_{7/2}}{4neF_2^2}, \quad (2)$$

in which the zero of energy is at the top of the valence band, and the energy is taken as positive as one descends into the valence band. To perform the model calculation, we first estimated  $E_F = 700$  K from the thermopower measurements (to be discussed below), and then adjusted  $m^*$  until the calculation agreed in magnitude with the data ( $m^* = 0.011m_e$ ). At 150 K, the model calculation predicts a carrier density  $n = 6.4 \times 10^{16} \text{ cm}^{-3}$ ; this can be compared to the Hall number,  $n_H = 1/R_H e = 7.0 \times 10^{16} \text{ cm}^{-3}$ . The good agreement between the temperature dependence of our model calculation and the temperature

dependence of the data strongly supports our identification of region 2 as the exhaustion regime, and ionized impurity scattering as the dominant scattering mechanism.

In a study of more heavily doped samples from room temperature to 500°C, Caillat, Borshcevsy, and Fleurial<sup>11</sup> estimated an effective mass of  $0.16m_e$ , using the assumption that acoustic-phonon scattering predominates. If, in our model calculations, we also assume acoustic lattice scattering, then we too would estimate a much larger effective mass. However, in our samples the temperature dependence of the Hall mobility clearly indicates ionized impurity scattering. Furthermore, whereas model calculations performed assuming ionized impurity scattering model the data quite well, calculations performed assuming acoustic-phonon scattering (or even neutral impurity scattering) do not even agree qualitatively with the data.

In Fig. 4, we plot the Hall mobility  $R_H/\rho$  vs temperature. We also plot a mobility that varies as  $T^{3/2}$ , which holds for scattering from ionized impurities.<sup>18</sup> Below 200 K, the data obey a  $T^{3/2}$  dependence reasonably well; above 200 K there is a crossover region, and the mobility begins to decrease with temperature, which most likely is due to the sudden influence of electrons on the Hall coefficient as the intrinsic regime is entered. It is also possible that the dominant scattering mechanism changes from ionized impurity scattering [ $\mu(T) \sim T^{3/2}$ ] to acoustic-phonon scattering [ $\mu(T) \sim T^{-3/2}$ ]. If we extrapolate the  $T^{3/2}$  behavior of the mobility to 300 K, we find that the mobility would be about  $3300 \text{ cm}^2 \text{ V}^{-1} \text{ s}^{-1}$ . This value is in good agreement with a sample measured by Caillat, Borshcevsy, and Fleurial<sup>11</sup> with a room-temperature Hall number  $n_H = 4 \times 10^{17}$  and mobility  $\mu = 3445.5 \text{ cm}^2 \text{ V}^{-1} \text{ s}^{-1}$ . If we compare these values with the values measured by Caillat, Borshcevsy, and Fleurial<sup>11</sup> on more heavily doped samples ( $n_H \approx 5 \times 10^{18}$ ,  $\mu \approx 1900 \text{ cm}^2 \text{ V}^{-1} \text{ s}^{-1}$ ), we find that there appears to be a strong dependence of the Hall mobility on carrier concentration, but there is as yet insufficient data to estimate precisely how the mobility varies with carrier concentration.

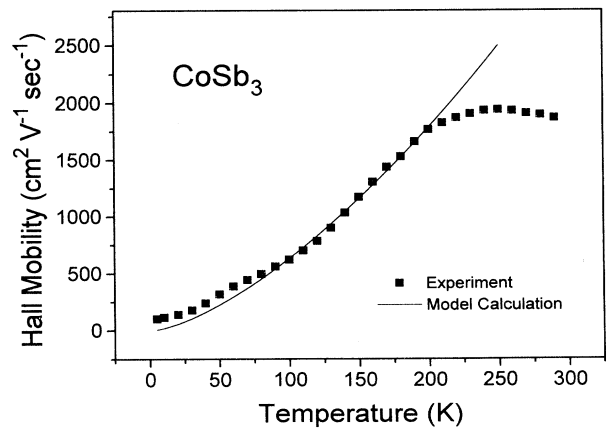


FIG. 4. Hall mobility  $R_H/\rho$  vs temperature for CoSb<sub>3</sub>. The solid line represents a  $T^{3/2}$  dependence, a signature of ionized impurity scattering.

In Fig. 5 we plot the Seebeck coefficient as a function of temperature for CoSb<sub>3</sub> (solid line). The overall shape of the data resembles that expected for ionized impurity scattering, and to illustrate this we also plot in Fig. 5 a model calculation of the Seebeck coefficient (dashed line). For the model calculation, we again assume a parabolic band, ionized impurity scattering, and hole conduction. For these assumptions, the Seebeck coefficient is given by<sup>17</sup>

$$S = \frac{k_B}{e} \left( \frac{4F_3}{3F_2} - E_F^* \right), \quad (3)$$

where  $E_F^* = E_F/T$ , and  $F_m$  are Fermi-Dirac integrals. For this calculation, we took a value of  $E_F = 700$  K, which was chosen to achieve the best qualitative agreement with the data; this value was used in calculating the Hall coefficient (see above). Although the agreement between the data and the calculation is only fair, it is probably the best that can be hoped for given that the bands in CoSb<sub>3</sub> are expected to be quasilinear<sup>3</sup> and not parabolic.

## V. CONCLUSIONS

In summary, we have grown single crystals of CoSb<sub>3</sub> from an Sb flux, and have performed a detailed structural refinement on them using powder-diffraction methods. We also have measured the resistivity, Hall coefficient, and Seebeck coefficient on a very lightly doped ( $n_H = 7.0 \times 10^{16}$  holes/cm<sup>3</sup>) single crystal. We have observed a semiconducting low-temperature resistivity in CoSb<sub>3</sub>, and have inferred a semiconducting energy gap of 580 K based on an Arrhenius plot of the resistivity. This observation verifies a key prediction of a recent band-structure calculation performed by Singh and Pickett.<sup>3</sup> A second, higher-energy scale ( $E_g \approx 0.31$  eV) was also observed, and this is also reasonably consistent with the pseudogap predicted in Ref. 3. The temperature dependence of the resistivity, Hall coefficient, and Seebeck coefficient clearly reflects the dominance of ionized impurity scattering. The effective mass of the carriers was

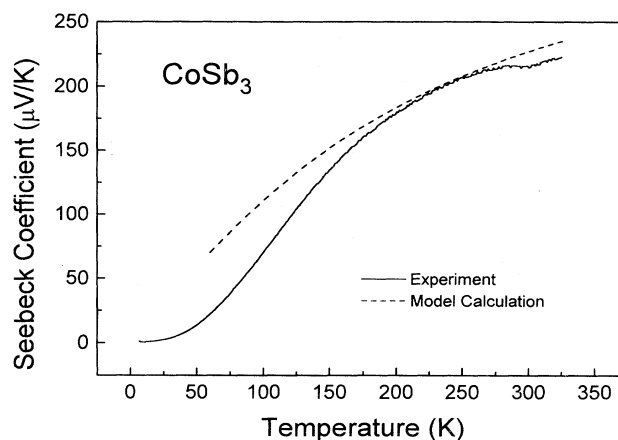


FIG. 5. Seebeck coefficient vs temperature for CoSb<sub>3</sub>. The dashed line represents a model calculation assuming a single type of carrier, parabolic bands, and scattering from ionized impurities (see text).

estimated to be  $0.011m_e$ ; this estimate is more than an order of magnitude smaller than estimates made assuming lattice scattering. Finally, although there is some evidence that the mobility increases with decreasing carrier concentration, we were unable to confirm the  $\mu \sim n^{-1/3}$  dependence predicted by Singh and Pickett.<sup>3</sup> Also, the presence of ionized impurity scattering did not allow us to test Singh and Pickett's expression for the thermopower, which was calculated assuming a temperature-independent scattering rate.

*Note added in proof.* After submission, the authors became aware of two recent works concerning CoSb<sub>3</sub>.<sup>19,20</sup>

## ACKNOWLEDGMENTS

We thank T. Bell for helping to construct the high-temperature resistivity apparatus, and A. Eklund for writing the data acquisition software used for the Hall effect measurements. The work at Los Alamos was performed under the auspices of the U.S. Department of Energy.

<sup>1</sup>T. Caillat, A. Borshchevsky, and J.-P. Fleurial, in *Proceedings of the Eleventh International Conference on Thermoelectrics, Arlington, Texas*, edited by K. R. Rao (University of Texas at Arlington Press, Arlington, 1993).  
<sup>2</sup>J.-P. Fleurial, T. Caillat, and Alex Borshchevsky, in *Thirteenth International Conference on Thermoelectrics*, edited by B. Mathiprakasham and P. Heenan, AIP Conf. Proc. No. 316 (AIP, New York, 1995).  
<sup>3</sup>D. J. Singh and Warren E. Pickett, *Phys. Rev. B* **50**, 11 235 (1994).  
<sup>4</sup>G. A. Slack and V. G. Tsoukala, *J. Appl. Phys.* **76**, 1665 (1994).  
<sup>5</sup>Z. Fisk and J. P. Remeika, in *Handbook on the Physics and Chemistry of Rare Earths*, edited by K. A. Gschneidner, Jr. and L. Eyring (Amsterdam, Elsevier, 1989), Vol. 12, p. 53.  
<sup>6</sup>W. B. Pearson, *The Crystal Chemistry and Physics of Metals and Alloys* (Wiley, New York, 1972).

<sup>7</sup>A. C. Larson and R. B. von Dreele (unpublished).  
<sup>8</sup>Th. Schmidt, G. Kliche, and H. D. Lutz, *Acta Crystallogr. Sect. C* **43**, 1678 (1987).  
<sup>9</sup>A. Kjekshus and T. Rakke, *Acta Chem. Scand. A* **28**, 99 (1974).  
<sup>10</sup>L. D. Dudkin and N. K. Abrikosov, *Zh. Neorg. Khim.* **1**, 2096 (1956) [*Russ. J. Inorg. Chem.* **1**, 169 (1956)].  
<sup>11</sup>T. Caillat, Alex Borshchevsky, and J.-P. Fleurial, in *Thirteenth International Conference on Thermoelectrics* (Ref. 2).  
<sup>12</sup>J. Ackermann and A. Wold, *J. Phys. Chem. Solids* **38**, 1013 (1977).  
<sup>13</sup>J.-P. Fleurial, in *Thirteenth International Conference on Thermoelectrics* (Ref. 2).  
<sup>14</sup>K. Matsubara, T. Iyanaga, T. Tsubouchi, K. Kishimoto, and T. Koyanagi, in *Thirteenth International Conference on Thermoelectrics* (Ref. 2).  
<sup>15</sup>E. H. Putley, *The Hall Effect and Related Phenomena* (Butter-

- worthington, London, 1960).
- <sup>16</sup>B. I. Shklovskii and A. L. Efros, *Electronic Properties of Doped Semiconductors* (Springer-Verlag, Berlin, 1984).
- <sup>17</sup>D. R. Lovett, *Semimetals & Narrow-Bandgap Semiconductors* (Pion Limited, London, 1977).
- <sup>18</sup>F. J. Blatt, in *Solid State Physics*, edited by F. Seitz and D. Turnbull (Academic, New York, 1957), Vol. 4, p. 200.
- <sup>19</sup>D. T. Morelli, T. Caillat, J.-P. Fleurial, A. Borshevsky, J. Vandersande, B. Chen, and C. Uher, *Phys. Rev. B* **51**, 9622 (1995).
- <sup>20</sup>J. W. Sharp, E. C. Jones, R. K. Williams, P. M. Martin, and B. C. Sales (unpublished).